

# **The Effect of pH on PAMAM Dendrimer-siRNA Complexation – Endosomal Considerations as Determined by Molecular Dynamics Simulation**

Defang Ouyang<sup>1</sup>, Hong Zhang<sup>2</sup>, Harendra S. Parekh<sup>3\*</sup> and Sean C. Smith<sup>2\*</sup>

<sup>1</sup>Aston University,

School of Life & Health Sciences

Birmingham B4 7ET, UK

<sup>2</sup>The University of Queensland,

Australian Institute of Bioengineering and Nanotechnology,

Centre for Computational Molecular Science,

Brisbane, QLD 4072, Australia

<sup>3</sup>The University of Queensland,

School of Pharmacy,

Brisbane, QLD 4072, Australia

\*Corresponding authors:

S.C. Smith      Tel: +61-7-3346 3949; Fax: +61-7-3346-3992; Email: [s.smith@uq.edu.au](mailto:s.smith@uq.edu.au)

H.S. Parekh      Tel: +61-7-3365 7430; Fax: +61-7-3365 1688; Email: [h.parekh@uq.edu.au](mailto:h.parekh@uq.edu.au)

Submitted to <Biophysical Chemistry>, April 2011

## **ABSTRACT**

Intracellular degradation of genes, most notably within the endo-lysosomal compartment is considered a significant barrier to (non-viral) gene delivery *in vivo*. Previous reports based on *in vitro* studies claim that carriers possessing a mixture of 1°, 2° & 3° amines are able to buffer the acidic environment within the endosome, allowing for timely release of their contents, leading to higher transfection rates. In this report, we adopt an atomistic molecular dynamics (MD) simulation approach, comparing the complexation of 21-bp siRNA with low-generation polyamidoamine (PAMAM) dendrimers (G0 and G1) at both neutral and acidic pHs, the latter of which mimics the degradative environment within maturing ‘late-endosomes’. Our simulations reveal that the time taken for the dendrimer-gene complex (dendriplex) to reach equilibrium is appreciably longer at low pH and this is accompanied by more compact packaging of the dendriplex, as compared to simulations performed at neutral pH. We also note higher calculated binding free energies of the dendriplex at low pH, indicating a higher dendrimer-gene affinity in comparison with neutral pH. These novel simulations provide a more detailed understanding of low molecular-weight polymer-siRNA behaviour, mimicking the endosomal environment and provide input of direct relevance to the “proton sponge theory”, thereby advancing the rational design of non-viral gene delivery systems.

### **Keywords:**

gene delivery, molecular dynamics simulation, dendrimer, proton sponge theory, siRNA, endosome

## 1. Introduction

The challenge of engineering into the design of vectors functionalities that facilitate the rapid escape of genes from endo-lysosomal degradation remains a major challenge in non-viral based gene delivery.<sup>1-3</sup> After cellular internalization of vector-gene complexes, they are captured into endosomal vesicles. Once inside the pH of the compartment rapidly decreases until a pH ~ 4 is reached, this then triggers fusion of the now “late-endosome” with lysosomes and the release a barrage of degradative enzymes. The process outlined above describes just one of the many inherent mechanisms present and necessary to protect cells invaded by potentially harmful (foreign) matter. One avenue to overcoming this barrier was first proposed by Behr J. P. in 1997 and has become widely accepted as the “proton sponge theory”.<sup>4</sup> The theory proposes that cationic carriers possessing internal 2° & 3° amines can counteract endosome acidification (via H<sup>+</sup> influx) as they buffer/capture H<sup>+</sup> ions to just below physiological pH, this delays lysosomal fusion to the endosome – an event that would ordinarily lead to degradation of the gene. This delay enables counterions (e.g. Cl<sup>-</sup> & H<sub>2</sub>O) to flood the endosomes, restoring the electronic balance, however vesicular-swelling results in their rupture and emptying of the contents, along with the vector-gene complexes, into the cytoplasm.<sup>5</sup> Another plausible explanation is that the gyration radius of a charged dendrimer increases with decreasing pH, as it gradually adopts an extended conformation, and this phenomenon may also contribute to timely endosomal rupture.<sup>6</sup> Recent simulation studies also confirm higher hydration radii of dendrimers in low pH versus neutral pH.<sup>6, 7</sup> An alternative *in-silico* model predicted that only a limited proportion of free versus cargo-bound polymer in the vesicles could impart endosomal membrane rupture upon decreasing pH<sup>8</sup>. This highlights that there are a multitude of factors at play here, and that detailed studies are necessary to further decipher the mechanism of polymer-induced endosomal rupture.<sup>9</sup> The

most common carriers known to overcome endosomal degradation include PAMAM dendrimer<sup>10, 11</sup>, poly(L-histidine)<sup>12-16</sup>, polyethylenimine (PEI)<sup>17-19</sup> and imidazole-containing polymers<sup>20-22</sup> as they possess 1°, 2° and 3° amine functionalities that effectively buffer the endosome. Although a number of reports have addressed biological aspects of endosomal escape, the impact of varying pH on the physical behaviour and dynamics displayed by vector-gene complexes while in the endosome is still unknown.

Direct experimental studies tracking the intracellular fate of gene-carrier complexes are very sparse due to the significant technical difficulties of such an undertaking. To-date only a handful of theoretical studies have attempted to elucidate gene-polycation behavior at pHs present within endosome. Maiti *et al.* studied the structure and dynamics of single-strand DNA-PAMAM dendrimer complexation in pH 7 and 4 by atomistic MD simulations.<sup>23</sup> The results indicated that PAMAM-DNA complexes at low pH are more loosely bound than those at neutral pH value. There are also considerable reported differences in the size and stability of complexes formed from double-strand versus single-strand genes, with the latter showing greater stability and smaller particle size under physiological (salt) conditions.<sup>24</sup> Studies using a simple mathematical model of the proton sponge effect (based on the Poisson-Boltzmann approach) prove the feasibility of the “proton sponge theory”.<sup>8</sup> The findings also suggest that a correlation exists between the amount of carrier and nucleic acid in any complex and that this in turn plays a role in the ability to induce membrane rupture upon decreasing pH, as is observed in the late-endosome.

In this study, we explore the complexation between a 21 base-pair duplex small interfering RNA (siRNA) and low-generation PAMAM dendrimers (G0 and G1 as shown in Figure S-1 Supporting Information) via atomistic MD simulations at two pHs mimicking the

environments of early (pH 7.0) and late (pH 5.0) endosomes. The significant toxicity imparted by higher-generation dendrimers (G4-G8) is widely accepted.<sup>25</sup> We therefore chose to simulate negligibly toxic, low-generation dendrimers, given their improved biocompatibility.<sup>25</sup> We go on to assess how both siRNA and carrier behave in these respective environments, which they are purported to be exposed to while in the endosome. Binding free energies of their complexation are estimated by the MM-PBSA method<sup>26-31</sup> in AMBER9<sup>32-34</sup> and are discussed in relation to structure and dynamical properties of the siRNA and their polycationic carriers.

## 2. Simulation Details

### 2.1 Molecular dynamics (MD) simulations

The sequence of the 21 base pair siRNA is taken from the earlier study by Putral *et al*<sup>35</sup> and is as follows:

Sense        5'- GCAACAGUUACUGCGACGUUU-3'  
Antisense    3'- UUCGUUGUCAAUGACGCUGCA -5'

The MD simulations utilize the AMBER9 software package<sup>32-34</sup> with the all-atom ff99 force field for RNA<sup>36</sup> and the general AMBER force field (gaff) for all polymers<sup>37</sup>. Duplex RNA was generated by the Nucleic Acid Builder (NAB) (<http://csegroup.rutgers.edu/>). All polymers were built by Material Studio 4.3 (<http://accelrys.com/products/materials-studio/>). At neutral pH (pH ~ 7), all the primary amines (4 for G0 and 8 for G1), while at low pH (pH ~ 5) all the primary and tertiary amines (6 for G0 and 14 for G1) are protonated. Using the LEAP module in AMBER 9, the polymer was positioned in the major groove or minor groove of RNA. The electrostatic interactions were calculated with the particle mesh Ewald method<sup>38-43</sup> and the cutoff was 10 Å. Using the LEAP module in AMBER 9, the complex

structure was immersed in a truncated octahedral water box with a solvation shell of 10 Å thickness using TIP3P model for water<sup>44</sup>. In addition, some water molecules were replaced by Na<sup>+</sup> counter-ions to neutralize the negative charge on the phosphate backbone of the RNA structure. This procedure resulted in solvated water structures containing approximately 30 000 atoms which included the 1335 RNA atoms and either 26 or 34 counter-ions (Na<sup>+</sup>), with the remainder being water molecules. The composition of these systems is shown in Table 1.

The minimization procedure for solvated complex consisted of two steps. In the first stage, the complex was kept fixed and positions of the water and ions were minimized. The solvated structures were then subjected to 1000 steps of steepest descent minimization followed by 1000 steps of conjugate gradient minimization.<sup>45, 46</sup> During this minimization process the complex was kept fixed in its starting conformation using harmonic constraints with a force constant of 500 kcal/mol/Å<sup>2</sup>. In the second stage, the entire system was minimized by 2000 steps of steepest descent minimization followed by 8000 steps of conjugate gradient minimization without the restraints.

The minimized structure was then subjected to 20 ps of MD, using a 2 fs time step for integration. During the MD simulation the system was gradually heated from 0 to 300 K using 10 kcal/mol/Å<sup>2</sup> weak positional restraints on the complex. The SHAKE algorithm was used in which all bonds involving hydrogen are constrained.<sup>47</sup> After the system was heated at constant volume with weak restraints on the complex, MD was performed for 20 ns with a time step of 2 fs under constant pressure/constant temperature (NPT ensemble) at 300 K with an average pressure of 1 atm without positional restraints. The random number seed of every restart was changed.<sup>48</sup> Isotropic position scaling<sup>49</sup> was used to maintain the pressure and a relaxation time of 2 ps was employed. SHAKE was used to constrain bonds involving

hydrogen and the temperature was kept at 300 K with Langevin dynamics<sup>50</sup> using a collision frequency of 1.0 ps<sup>-1</sup>.

## 2.2 MM-PBSA Free Energy Calculations

The binding free energy for each complex was calculated using the MM-PBSA method in AMBER 9.<sup>26-31</sup> In this method the average interaction energies of the receptor and the ligand were calculated using an ensemble of snapshot structures taken from the MD trajectory of the system. The binding free energy in solution ( $\Delta G_{\text{bind}}$ ) was computed from the solvation free energies for the receptor, the ligand and the complex [ $\Delta G_{\text{water}}(\text{receptor})$ ,  $\Delta G_{\text{water}}(\text{ligand})$  and  $\Delta G_{\text{water}}(\text{complex})$ ]:

$$\Delta G_{\text{bind}} = \Delta G_{\text{water}}(\text{complex}) - [\Delta G_{\text{water}}(\text{receptor}) + \Delta G_{\text{water}}(\text{ligand})] \quad (1)$$

The free energies for each species (the receptor, the ligand and the complex),  $\Delta G_{\text{water}}$ , were calculated using the following equations:

$$\Delta G_{\text{water}} = E_{\text{MM}} + G_{\text{solvation}} - TS \quad (2)$$

$$G_{\text{solvation}} = G_{\text{PB}} + G_{\text{nonpolar}} \quad (3)$$

$$E_{\text{MM}} = E_{\text{internal}} + E_{\text{electrostatic}} + E_{\text{vdW}} \quad (4)$$

$$E_{\text{internal}} = E_{\text{bond}} + E_{\text{angle}} + E_{\text{torsion}} \quad (5)$$

where  $E_{\text{MM}}$  is the absolute molecular mechanical energy;  $G_{\text{solvation}}$  is the solvation free energy;  $G_{\text{PB}}$  is the electrostatic solvation free energy;  $G_{\text{nonpolar}}$  is the nonpolar solvation free energy;  $E_{\text{electrostatic}}$  and  $E_{\text{vdW}}$  are the electrostatic and Van der Waals interaction energy, respectively; the internal energy  $E_{\text{internal}}$  is determined by  $E_{\text{bond}}$ ,  $E_{\text{angle}}$  and  $E_{\text{torsion}}$ , which represent the strain energy in bonds, angles and torsion angles;  $T$  is the temperature and  $S$  is the entropy.

The entropy contributions were determined by the NMODE program within AMBER, but in practice these values are ignored because different polymer to the same nucleic acid shows similar entropy for a comparison of states and their calculations need quite costly computing

abilities.  $E_{MM}$  from each snapshot was calculated using the ANAL program of AMBER with all pair-wise interactions included using a dielectric constant ( $\epsilon$ ) of 1.  $E_{internal}$  always amounts to zero in the single trajectory approach. The solvation free energy ( $G_{solvation}$ ) was estimated by two different approaches: the Poisson–Boltzmann finite-difference equation (FDPB)<sup>51-53</sup> and the generalized Born approach (GB)<sup>54-59</sup>.

We used  $\epsilon = 1$  for the solute and  $\epsilon = 80$  for the solvent in the electrostatic solvation free energy ( $\Delta G_{PB}$ ) calculations. A solvent probe radius of 1.4 Å was used for the molecular surface.<sup>60</sup> Atomic charges of the Cornell *et al.* force field were used for calculating the total electrostatic energies<sup>61</sup>. An 80% boxfill cubic lattice and a grid resolution of 0.5 Å/grid point were used in the PB calculations. The nonpolar contribution to the solvation free energy was determined with solvent-accessible-surface-area (SASA) terms with *molsurf* program.<sup>62, 63</sup> The *molsurf* program was used to calculate the nonpolar solvation free energy ( $G_{nonpolar}$ ) as follows:

$$G_{nonpolar} = SURFTEN * SASA + SURFOFF \quad (6)$$

where SURFTEN is 0.0072 kcal / Å and SURFOFF is 0 kcal/mol.<sup>60</sup>

Binding free energy calculations were performed using single polymer–RNA trajectories. This meant that the snapshot structures for the energy calculations of the polymer–RNA complex and separated polymer and RNA were taken from the unbound polymers, unbound RNA and the complexes. From the last two nanosecond of each equilibrated trajectory in 10 ps intervals, 200 snapshots were taken at even intervals for the binding energy analyses and the reported binding free energies are averages of the 200 snapshots.

### **3. Results and Discussions**

#### **3.1 Structural aspects of the complex**

Snapshots at 4 ns intervals from the 20 ns MD simulations are shown for the 14<sup>+</sup>dendrimer at low pH in Figures 1 and 2, compared to Figure 3, where the same dendrimer has only its head-group amines protonated (8<sup>+</sup>dendrimer) at neutral pH. Figure 1 is derived from a simulation in which the 14<sup>+</sup>dendrimer was initially positioned near the major groove at the middle of the strand, while Figure 2 relates to a simulation where the dendrimer was positioned near the minor groove at the middle of the strand. From these figures it is apparent that 14<sup>+</sup>dendrimer interacts more compactly with siRNA than 8<sup>+</sup>dendrimer on both major and minor grooves. Furthermore, from the snapshots of Figure 2, we can see that there are strong duplex-RNA deforming characteristics in the presence of polymer, with the polymer also making contact with the terminal phosphate groups of the RNA. However, one may observe that the cationic charge density of even our 8<sup>+</sup>polymer is not strong enough to enable the RNA molecule to fully wrap itself around the polymer. Our results differ from a previous 20 ns simulation study claiming loose high-generation PAMAM dendrimer-DNA association at low pH.<sup>23</sup> Here, the authors claim that the high generation of the dendrimer with more surface and internal charged basic (nitrogen) moieties attracts counterions e.g. Cl<sup>-</sup> ions towards the surface and interior of these positively charged dendrimers, which in turn neutralizes the net cationic charge density, thereby decreasing DNA-dendrimer binding affinity.<sup>23</sup> Moreover, it is very likely that differences in gene-architecture and length play a role in this disparity, between their single (38-bp) and our double strand (21-bp) gene simulations. However, even after taking this difference on board, another probable reason may be the inadequate sampling time and that big system was trapped at the local minima because a complex system needs more time to reach the equilibrium than a simple system, as we discuss later. Analogous

results for the PAMAM G0 6<sup>+</sup>dendrimer are shown in Figure S-2 (see Supporting Information). The 6<sup>+</sup>dendrimers all bind on the major groove of the siRNA, even when initially placed on the minor groove side of the nucleic acid, which is in accordance with our previous simulation data.<sup>64</sup> However, we observed that the system takes longer to reach equilibrium than the 4<sup>+</sup>dendrimers because 6<sup>+</sup>dendrimers need to overcome higher local energy barriers to reach the lowest energy minima (data not shown).

### 3.2 Dynamics of the complex formation

The root-mean-squared deviation (RMSD) plots for the polymer-RNA complexes are shown in Figure 4 and represent the fluctuation of atoms on the backbone of the 14<sup>+</sup> G1-RNA complexes. It is apparent that this parameter reaches a plateau and shows relative stability only after  $\sim$  15 ns, indicating that 14<sup>+</sup>G1-RNA systems are reasonably equilibrated after the timescale of 20 ns simulations, while 8<sup>+</sup>G1-RNA complexes reach the equilibrium more quickly after about 7 ns, as shown in Figure S-4. 6<sup>+</sup>G0-RNA complexation displays a similar rate of equilibration to that of 4<sup>+</sup>G0-RNA interactions, as shown in Figure S-3 and S-4 (Supporting Information). These observations further confirm that complex systems such as presently studied need more time to reach equilibrium than a simple system. In light of this, the previously reported simulations e.g. PAMAM G4 126<sup>+</sup>dendrimer / 37 base DNA spanning 20 ns simulation time may well fall short of the time necessary for such a complex system to reach equilibrium.<sup>23, 65</sup>

In agreement with the snapshots in Figure 1 and 2, as demonstrated in Figure 5, there is a significant decrease of RNA length during the simulation in the case where the starting position is adjacent to the minor groove of RNA. The reason here may be that the terminal ‘overhanging’ Uracil has added flexibility and with its proximity can wrap itself around the

dendrimer when the starting position is located adjacent to the minor groove of RNA. During MD simulations, as implied by the snapshots of Figures 1 and 2, our carriers gradually change their position and then merge with the gene. This process can be tracked by examining the numbers of close contacts between carrier and gene as the simulation proceeds. In Figure 6, the time dependence of the number of contacts between RNA and polymer is shown for the two simulations represented in Figures 1 and 2. It is apparent that in the later stage of the simulations, the contact number for the trajectory with the minor groove starting position is greater than that for the major groove starting position, which is consistent with the clearly observable bending of RNA around the polymer as shown in Fig.s 1, 2 and 5. Figure 7 shows the plot of the number of water molecules that are within 3 Å of the dendrimer versus time. It is apparent from Figure 7(a) that the number of solvating water molecules decreases significantly until the ~15 ns time point of the complexation process. Moreover, in the late stages of the simulation, shown more clearly in Figure 7(b), the number of water molecules within 3 Å of the dendrimer for the trajectory with the minor groove starting position is less than for the major groove starting position, confirming that more solvent molecules are squeezed out upon the bending of RNA around the dendrimer discussed above.

### 3.3 Binding free energies

We have estimated binding free energies for the range of carrier systems investigated using the methods summarized in Section 2 and the results are presented in Table 2. From these values, it is clear that electrostatic interactions play a primary role in the association of gene and dendrimer, in agreement with our previous simulations. For example, a value of 159.11/238.83 kcal/mol (~ 67%) can be attributed to the electrostatic-affinity of  $^{14+}$ dendrimer-RNA complex in the minor groove. These values further confirm previous

results that polycation-DNA or RNA complexation depends primarily on electrostatic interactions between the positively-charged carrier and the negatively-charged phosphate groups on the backbone of nucleic acids.

As electrostatic interaction is the major driving force in the overall complexation process, the binding energy for polyamine-based vectors at low pH should be higher than that at neutral pH. It is apparent from Table 2 that this is indeed the case with binding free energies for all simulated systems at low pH being higher than those calculated at neutral pH, e.g. 209.71 kcal/mol for 14<sup>+</sup>dendrimer-RNA complex initially adjacent to the major groove in comparison with 138.30 kcal/mol for 8+dendrimer-RNA complex adjacent to the major groove. The snapshots of Figure 1 and 2 also indirectly allude to this since complexes at low pH appear more compact than those observed at pH 7. Histidine-based polymers also show similar results to that of PAMAM dendrimers (data not shown). This suggests that polymer-gene complexes at low pH in the maturing late-endosome are more compact than in the general (cytosolic) cell environment at pH 7.

#### 4. Conclusions

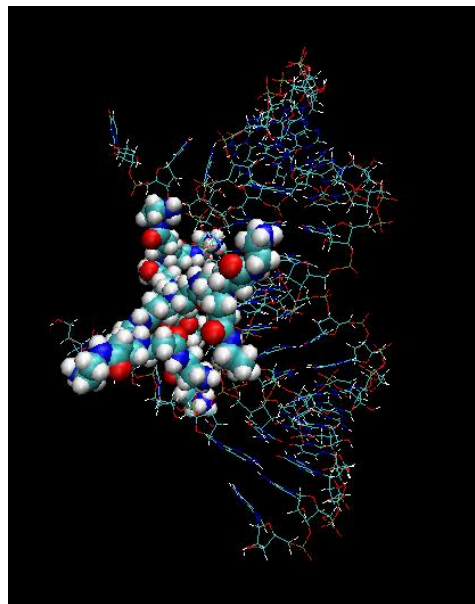
The present simulations provide us a detailed molecular level understanding of both structural and dynamical aspects of siRNA-low generation PAMAM dendrimer complexation within different pH environments of early and late-endosomes as proposed by the “proton sponge theory”. The complexes at low pH are more compact than those at neutral pH. The calculations of the binding free energy indicate that electrostatic attraction is the primary contributor to this interaction and that these energies are higher at low pH compared to at neutral pH. Hence, with detailed molecular modeling we are for the first time unraveling how low molecular-weight dendrimer-siRNA complexes behave in the low-pH environment of the

late-endosome. However, further studies are indeed necessary extend our understanding of the multi-faceted role endosomal-pH has to play in assisting the delivery of therapeutic cargo using generic polymeric gene vectors.

### **Acknowledgements**

We acknowledge generous allocations of CPU time from the Australian National Computing Infrastructure (NCI) facility and the computational molecular science cluster computing facility at The University of Queensland, funded in part by the Australian Research Council (ARC) Linkage, Infrastructure, Equipment and Facilities (LIEF) scheme (grant number LE0882357).

**Table of contents (TOC) Graphic**



This figure is the snapshot of  $14^+$ dendrimer complexed in the minor groove of RNA in 10 ns of MD simulation.

## References

1. Park, T. G.; Jeong, J. H.; Kim, S. W., Current status of polymeric gene delivery systems. *Adv. Drug Deliv. Rev.* **2006**, *58* (4), 467-86.
2. Read, M. L.; Logan, A.; Seymour, L. W., Barriers to gene delivery using synthetic vectors. *Adv. Genet.* **2005**, *53*, 19-46.
3. Cho, Y. W.; Kim, J. D.; Park, K., Polycation gene delivery systems: escape from endosomes to cytosol. *Journal of Pharmacy and Pharmacology* **2003**, *55* (6), 721-734.
4. Behr, J. P., The proton sponge: A trick to enter cells the viruses did not exploit. *Chimia* **1997**, *51* (1-2), 34-36.
5. Sonawane, N. D.; Szoka, F. C.; Verkman, A. S., Chloride accumulation and swelling in endosomes enhances DNA transfer by polyamine-DNA polyplexes. *Journal of Biological Chemistry* **2003**, *278* (45), 44826-44831.
6. Tian, W. D.; Ma, Y. Q., Coarse-grained molecular simulation of interacting dendrimers. *Soft Matter* **7** (2), 500-505.
7. Maiti, P. K.; Cagin, T.; Lin, S. T.; Goddard, W. A., Effect of solvent and pH on the structure of PAMAM dendrimers. *Macromolecules* **2005**, *38* (3), 979-991.
8. Yang, S.; May, S., Release of cationic polymer-DNA complexes from the endosome: A theoretical investigation of the proton sponge hypothesis. *Journal of Chemical Physics* **2008**, *129* (18).
9. Won, Y. Y.; Sharma, R.; Konieczny, S. F., Missing pieces in understanding the intracellular trafficking of polycation/DNA complexes. *Journal of Controlled Release* **2009**, *139* (2), 88-93.
10. Patil, M. L.; Zhang, M.; Taratula, O.; Garбуzenko, O. B.; He, H. X.; Minko, T., Internally Cationic Polyamidoamine PAMAM-OH Dendrimers for siRNA Delivery: Effect of the Degree of Quaternization and Cancer Targeting. *Biomacromolecules* **2009**, *10* (2), 258-266.
11. Parekh, H. S., The advance of dendrimers--a versatile targeting platform for gene/drug delivery. *Curr. Pharm. Des.* **2007**, *13* (27), 2837-50.
12. Midoux, P.; Kichler, A.; Boutin, V.; Maurizot, J. C.; Monsigny, M., Membrane permeabilization and efficient gene transfer by a peptide containing several histidines. *Bioconjugate Chem.* **1998**, *9* (2), 260-7.
13. Midoux, P.; Monsigny, M., Efficient gene transfer by histidylated polylysine/pDNA complexes. *Bioconjugate Chem.* **1999**, *10* (3), 406-11.
14. Leng, Q. X.; Goldgeier, L.; Zhu, J. S.; Cambell, P.; Ambulos, N.; Mixson, A. J., Histidine-lysine peptides as carriers of nucleic acids. *Drug News & Perspectives* **2007**, *20* (2), 77-86.
15. Mason, A. J.; Leborgne, C.; Moulay, G.; Martinez, A.; Danos, O.; Bechinger, B.; Kichler, A., Optimising histidine rich peptides for efficient DNA delivery in the presence of serum. *J. Controlled Release* **2007**, *118* (1), 95-104.
16. Asayama, S.; Kato, H.; Kawakami, H.; Nagaoka, S., Carboxymethyl poly(L-histidine) as a new pH-sensitive polypeptide at endosomal/lysosomal pH. *Polym. Adv. Technol.* **2007**, *18* (4), 329-333.
17. Seib, F. P.; Jones, A. T.; Duncan, R., Comparison of the endocytic properties of linear and branched PEIs, and cationic PAMAM dendrimers in B16f10 melanoma cells. *J. Controlled Release* **2007**, *117* (3), 291-300.
18. Cherrng, J. Y., Investigation of DNA Spectral Conformational Changes and Polymer Buffering Capacity in Relation to Transfection Efficiency of DNA/Polymer Complexes. *J. Pharm. Pharm. Sci.* **2009**, *12* (3), 346-356.
19. Akinc, A.; Thomas, M.; Klibanov, A. M.; Langer, R., Exploring polyethylenimine-mediated DNA transfection and the proton sponge hypothesis. *Journal of Gene Medicine* **2005**, *7* (5), 657-663.
20. Pack, D. W.; Putnam, D.; Langer, R., Design of imidazole-containing endosomolytic biopolymers for gene delivery. *Biotechnol. Bioeng.* **2000**, *67* (2), 217-223.
21. Ihm, J. E.; Han, K. O.; Han, I. K.; Ahn, K. D.; Han, D. K.; Cho, C. S., High transfection efficiency of poly(4-vinylimidazole) as a new gene carrier. *Bioconjugate Chem.* **2003**, *14* (4), 707-8.

22. Midoux, P.; Pichon, C.; Yaouanc, J. J.; Jaffres, P. A., Chemical vectors for gene delivery: a current review on polymers, peptides and lipids containing histidine or imidazole as nucleic acids carriers. *Brit. J. Pharmacol.* **2009**, *157* (2), 166-178.
23. Maiti, P. K.; Bagchi, B., Structure and dynamics of DNA-dendrimer complexation: Role of counterions, water, and base pair sequence. *Nano Lett.* **2006**, *6* (11), 2478-2485.
24. Molas, M.; Bartrons, R.; Perales, J. C., Single-stranded DNA condensed with poly-L-lysine results in nanometric particles that are significantly smaller, more stable in physiological ionic strength fluids and afford higher efficiency of gene delivery than their double-stranded counterparts. *Biochim. Biophys. Acta-Gen. Subjects* **2002**, *1572* (1), 37-44.
25. Shah N, S. R. J., Parekh H S, Low-generation asymmetric dendrimers exhibit minimal toxicity and effectively complex DNA. *Journal of Peptide Science* **2011**, DOI 10.1002/psc.1347.
26. Srinivasan, J.; Cheatham, T. E.; Cieplak, P.; Kollman, P. A.; Case, D. A., Continuum solvent studies of the stability of DNA, RNA, and phosphoramidate - DNA helices. *Journal of the American Chemical Society* **1998**, *120* (37), 9401-9409.
27. Kollman, P. A.; Massova, I.; Reyes, C.; Kuhn, B.; Huo, S. H.; Chong, L.; Lee, M.; Lee, T.; Duan, Y.; Wang, W.; Donini, O.; Cieplak, P.; Srinivasan, J.; Case, D. A.; Cheatham, T. E., Calculating structures and free energies of complex molecules: Combining molecular mechanics and continuum models. *Accounts of Chemical Research* **2000**, *33* (12), 889-897.
28. Kuhn, B.; Kollman, P. A., Binding of a diverse set of ligands to avidin and streptavidin: An accurate quantitative prediction of their relative affinities by a combination of molecular mechanics and continuum solvent models. *Journal of Medicinal Chemistry* **2000**, *43* (20), 3786-3791.
29. Lee, M. R.; Duan, Y.; Kollman, P. A., Use of MM-PB/SA in estimating the free energies of proteins: Application to native, intermediates, and unfolded villin headpiece. *Proteins-Structure Function and Genetics* **2000**, *39* (4), 309-316.
30. Massova, I.; Kollman, P. A., Combined molecular mechanical and continuum solvent approach (MM-PBSA/GBSA) to predict ligand binding. *Perspectives in Drug Discovery and Design* **2000**, *18*, 113-135.
31. Reyes, C. M.; Kollman, P. A., Structure and thermodynamics of RNA-protein binding: Using molecular dynamics and free energy analyses to calculate the free energies of binding and conformational change. *Journal of Molecular Biology* **2000**, *297* (5), 1145-1158.
32. Case, D. A.; Darden, T. A.; Cheatham, I., T.E. ; Simmerling, C. L.; Wang, J.; Duke, R. E.; Luo, R.; Merz, K. M.; Pearlman, D. A.; Crowley, M.; Walker, R. C.; Zhang, W.; Wang, B.; Hayik, S.; Roitberg, A.; Seabra, G.; Wong, K. F.; Paesani, F.; Wu, X.; Brozell, S.; Tsui, V.; Gohlke, H.; Yang, L.; Tan, C.; Mongan, J.; Hornak, V.; Cui, G.; Beroza, P.; Mathews, D. H.; Schafmeister, C.; Ross, W. S.; Kollman, P. A. *AMBER 9*, University of California: San Francisco, 2006.
33. Case, D. A.; Cheatham, T. E.; Darden, T.; Gohlke, H.; Luo, R.; Merz, K. M.; Onufriev, A.; Simmerling, C.; Wang, B.; Woods, R. J., The Amber biomolecular simulation programs. *Journal of Computational Chemistry* **2005**, *26* (16), 1668-1688.
34. Pearlman, D. A.; Case, D. A.; Caldwell, J. W.; Ross, W. S.; Cheatham, T. E.; Debolt, S.; Ferguson, D.; Seibel, G.; Kollman, P., AMBER, a package of computer-programs for applying molecular mechanics, normal-mode analysis, molecular-dynamics and free-energy calculations to simulate the structural and energetic properties of molecules. *Comput Phys Commun* **1995**, *91* (1-3), 1-41.
35. Putral, L. N.; Bywater, M. J.; Gu, W.; Saunders, N. A.; Gabrielli, B. G.; Leggatt, G. R.; McMillan, N. A., RNA interference against human papillomavirus oncogenes in cervical cancer cells results in increased sensitivity to cisplatin. *Mol. Pharmacol.* **2005**, *68* (5), 1311-9.
36. Wang, J. M.; Cieplak, P.; Kollman, P. A., How well does a restrained electrostatic potential (RESP) model perform in calculating conformational energies of organic and biological molecules? *Journal of Computational Chemistry* **2000**, *21* (12), 1049-1074.

37. Wang, J. M.; Wolf, R. M.; Caldwell, J. W.; Kollman, P. A.; Case, D. A., Development and testing of a general amber force field (vol 25, pg 1157, 2004). *Journal of Computational Chemistry* **2005**, *26* (1), 114-114.
38. Darden, T.; York, D.; Pedersen, L., Particle mesh ewald - an n.log(n) method for ewald sums in large systems. *J Chem Phys* **1993**, *98* (12), 10089-10092.
39. Essmann, U.; Perera, L.; Berkowitz, M. L.; Darden, T.; Lee, H.; Pedersen, L. G., A smooth particle mesh ewald method. *J Chem Phys* **1995**, *103* (19), 8577-8593.
40. Crowley, M. F.; Darden, T. A.; Cheatham, T. E.; Deerfield, D. W., Adventures in improving the scaling and accuracy of a parallel molecular dynamics program. *Journal of Supercomputing* **1997**, *11* (3), 255-278.
41. Sagui, C.; Darden, T. A. In *P3M and PME: a comparison of the two methods*, Workshop on Treatment of Electrostatic Interactions in Computer Simulations of Condensed Media, Santa Fe, Nm, Jun 23-25; Pratt, L. R.; Hummer, G., Eds. Santa Fe, Nm, 1999; pp 104-113.
42. Toukmaji, A.; Sagui, C.; Board, J.; Darden, T., Efficient particle-mesh Ewald based approach to fixed and induced dipolar interactions. *J Chem Phys* **2000**, *113* (24), 10913-10927.
43. Sagui, C.; Pedersen, L. G.; Darden, T. A., Towards an accurate representation of electrostatics in classical force fields: Efficient implementation of multipolar interactions in biomolecular simulations. *J Chem Phys* **2004**, *120* (1), 73-87.
44. Jorgensen, W. L.; Chandrasekhar, J.; Madura, J. D.; Impey, R. W.; Klein, M. L., Comparison of simple potential functions for simulating liquid water. *J Chem Phys* **1983**, *79* (2), 926-935.
45. Leach, A. R., *Molecular modelling: principles and applications*. 2nd ed.; Prentice Hall: 2001.
46. Hans-Dieter Höltje; Wolfgang Sippl; Didier Rognan; Folkers, G., *Molecular Modeling: Basic Principles and Applications* 3rd ed.; Weinheim : Wiley-VCH: 2008.
47. Ryckaert, J. P.; Ciccotti, G.; Berendsen, H. J. C., Numerical-integration of cartesian equations of motion of a system with constrains - molecular dynamics of n-alkanes. *J Comput Phys* **1977**, *23* (3), 327-341.
48. Cerutti, D. S.; Duke, R.; Freddolino, P. L.; Fan, H.; Lybrand, T. P., A Vulnerability in Popular Molecular Dynamics Packages Concerning Langevin and Andersen Dynamics. *Journal of Chemical Theory and Computation* **2008**, *4* (10), 1669-1680.
49. Berendsen, H. J. C.; Postma, J. P. M.; Vangunsteren, W. F.; Dinola, A.; Haak, J. R., Molecular dynamics with coupling to an external bath. *J Chem Phys* **1984**, *81* (8), 3684-3690.
50. Wu, X. W.; Brooks, B. R., Self-guided Langevin dynamics simulation method. *Chemical Physics Letters* **2003**, *381* (3-4), 512-518.
51. Luo, R.; David, L.; Gilson, M. K., Accelerated Poisson-Boltzmann calculations for static and dynamic systems. *Journal of Computational Chemistry* **2002**, *23* (13), 1244-1253.
52. Lu, Q.; Luo, R., A Poisson-Boltzmann dynamics method with nonperiodic boundary condition. *J Chem Phys* **2003**, *119* (21), 11035-11047.
53. Honig, B.; Nicholls, A., CLASSICAL ELECTROSTATICS IN BIOLOGY AND CHEMISTRY. *Science (New York, N.Y)* **1995**, *268* (5214), 1144-1149.
54. Still, W. C.; Tempczyk, A.; Hawley, R. C.; Hendrickson, T., SEMIANALYTICAL TREATMENT OF SOLVATION FOR MOLECULAR MECHANICS AND DYNAMICS. *Journal of the American Chemical Society* **1990**, *112* (16), 6127-6129.
55. Jayaram, B.; Sprous, D.; Beveridge, D. L., Solvation free energy of biomacromolecules: Parameters for a modified generalized born model consistent with the AMBER force field. *Journal of Physical Chemistry B* **1998**, *102* (47), 9571-9576.
56. Cramer, C. J.; Truhlar, D. G., Implicit solvation models: Equilibria, structure, spectra, and dynamics. *Chemical Reviews* **1999**, *99* (8), 2161-2200.
57. Bashford, D.; Case, D. A., Generalized born models of macromolecular solvation effects. *Annual Review of Physical Chemistry* **2000**, *51*, 129-152.
58. Onufriev, A.; Bashford, D.; Case, D. A., Modification of the generalized Born model suitable for macromolecules. *Journal of Physical Chemistry B* **2000**, *104* (15), 3712-3720.

59. Lee, M. S.; Salsbury, F. R.; Brooks, C. L., Novel generalized Born methods. *J Chem Phys* **2002**, *116* (24), 10606-10614.
60. AMBER, AMBER 9 Users' Manual. <http://ambermd.org/doc9/>: 2007.
61. Cornell, W. D.; Cieplak, P.; Bayly, C. I.; Gould, I. R.; Merz, K. M.; Ferguson, D. M.; Spellmeyer, D. C.; Fox, T.; Caldwell, J. W.; Kollman, P. A., A 2nd generation force field for the simulation of proteins, nucleic acids, and organic molecules. *J. Am. Chem. Soc.* **1995**, *117* (19), 5179-5197.
62. Sitkoff, D.; Sharp, K. A.; Honig, B., ACCURATE CALCULATION OF HYDRATION FREE-ENERGIES USING MACROSCOPIC SOLVENT MODELS. *J Phys Chem-US* **1994**, *98* (7), 1978-1988.
63. Connolly, M. L., ANALYTICAL MOLECULAR-SURFACE CALCULATION. *Journal of Applied Crystallography* **1983**, *16* (OCT), 548-558.
64. Ouyang, D. F.; Zhang, H.; Herten, D. P.; Parekh, H. S.; Smith, S. C., Structure, dynamics, and energetics of siRNA-cationic vector complexation: a molecular dynamics study. *J. Phys. Chem. B* **2010**, *114* (28), 9220-9230.
65. Pavan, G. M.; Albertazzi, L.; Danani, A., Ability to Adapt: Different Generations of PAMAM Dendrimers Show Different Behaviors in Binding siRNA. *Journal of Physical Chemistry B* **114** (8), 2667-2675.

## **Figures**

Figure 1 Snapshots of the  $14^+G1$  complexed with RNA when the starting position is adjacent to the major groove: a) at 0 ns; b) after 4 ns; c) after 8 ns; d) after 12 ns; e) after 16 ns; f) after 20 ns.

Figure 2 Snapshots of the  $14^+G1$  complexed with RNA when the starting position is adjacent to the minor groove: a) at 0 ns; b) after 4 ns; c) after 8 ns; d) after 12 ns; e) after 16 ns; f) after 20 ns.

Figure 3 Snapshots of  $8^+G1$  complexed with RNA at 18 ns (a) the starting positions on the minor groove of RNA; b) the starting positions on the major groove of RNA.

Figure 4 RMSD versus time of 14+G1-RNA complexation in 20 ns simulation

Figure 5. RNA length as a function of time for complexation between 14+G1 and RNA during the 20 ns simulations.

Figure 6 Variation of the number of contact points between 14+G1 and RNA (any contact within 3 Å) in 20 ns simulation

Figure 7 Number of water molecules in a spine of hydration (within 3 Å of the polymer) as a function of time between 14+G1 and RNA (any contact within 3 Å) in 20 ns simulation.

## Tables

Table 1 Simulations cell compositions and atom numbers for the systems of cationic polymers-siRNA complexation

Table 2 Binding free energies for polymer-RNA complex in the minor or major groove using the MM-PBSA method

## **Supplementary Materials**

Figure S-1 Chemical structures of polymers

Figure S-2 Snapshots of 6<sup>+</sup>G0 complexed with RNA on 20 ns with different starting position

Figure S-3 RMSD versus time for 6+G0-RNA complexation over the 20 ns simulations

Figure S-4 RMSD versus time of dendrimer-RNA complexation in 18 ns at neutral pH.

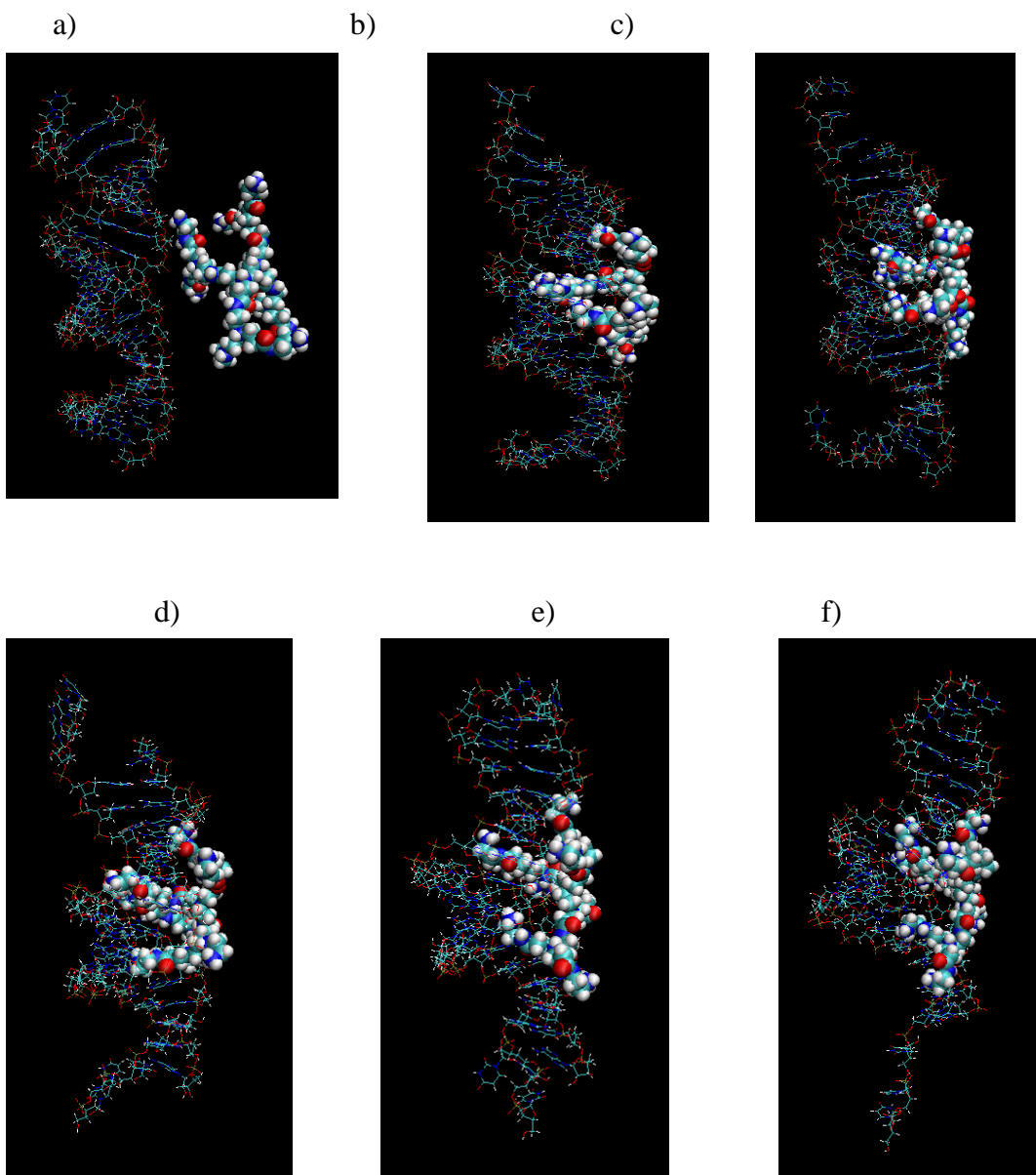


Figure 1 Snapshots of the 14<sup>+</sup>G1 complexed with RNA when the starting position is adjacent to the major groove: a) at 0 ns; b) after 4 ns; c) after 8 ns; d) after 12 ns; e) after 16 ns; f) after 20 ns.

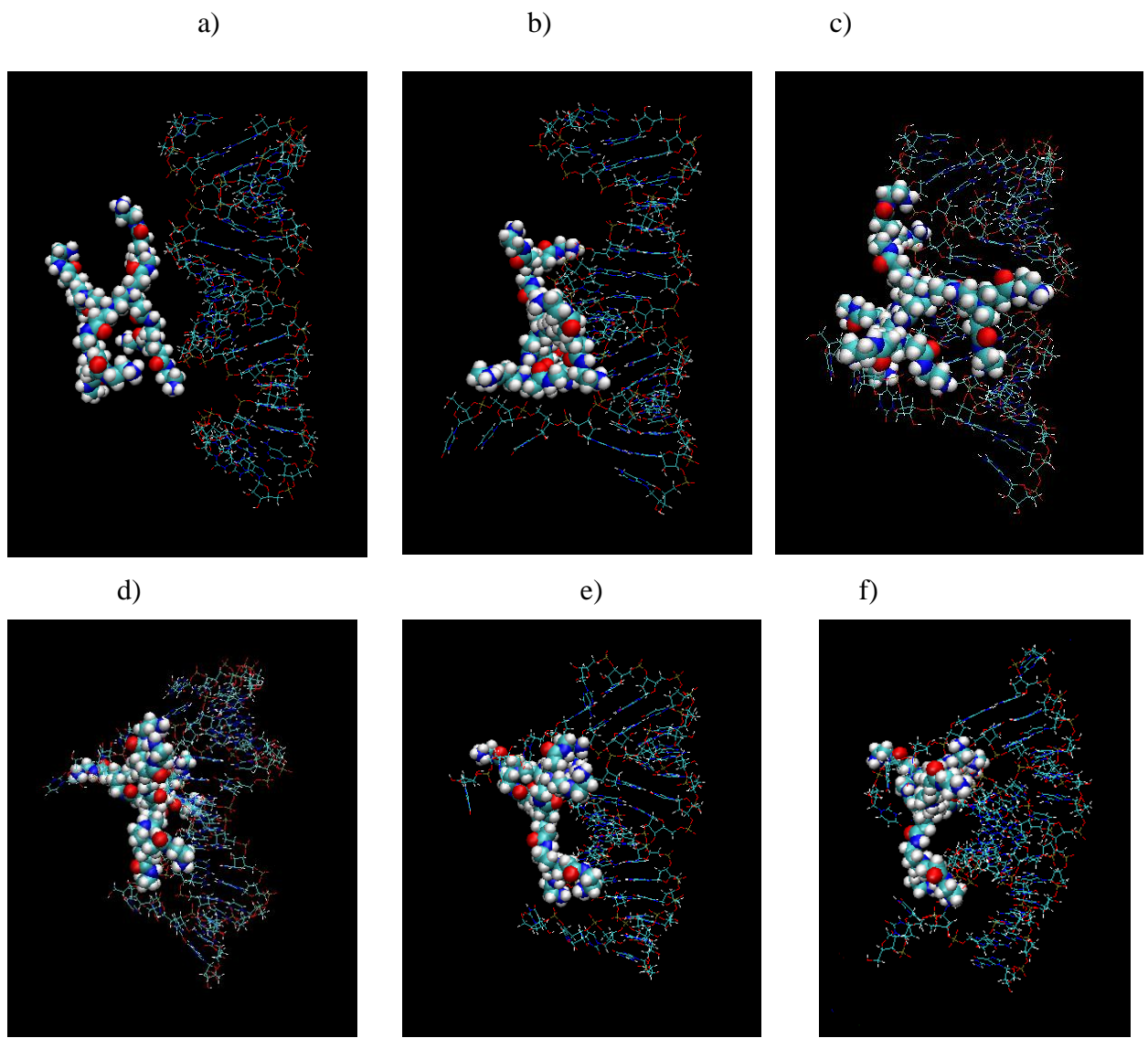


Figure 2 Snapshots of the  $14^+G1$  complexed with RNA when the starting position is adjacent to the minor groove: a) at 0 ns; b) after 4 ns; c) after 8 ns; d) after 12 ns; e) after 16 ns; f) after 20 ns.

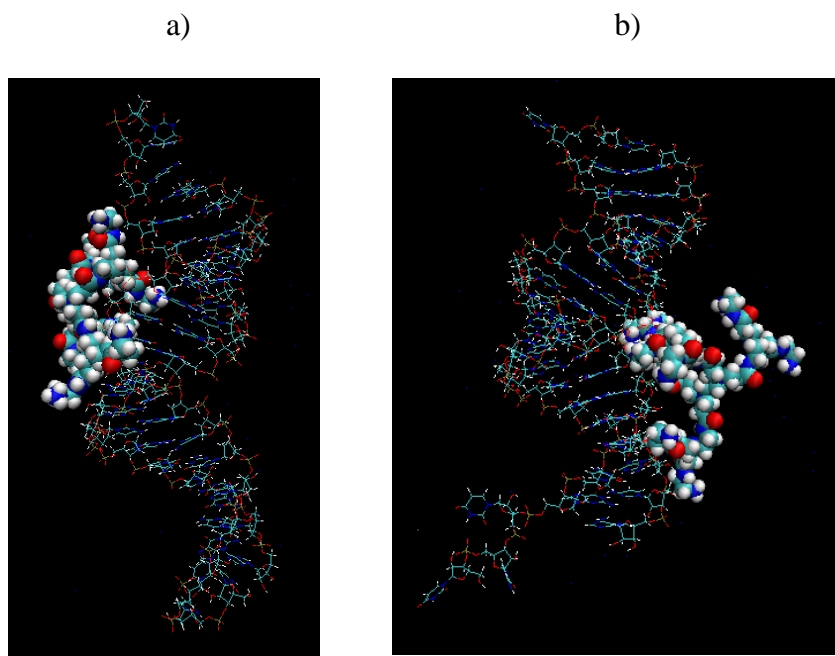


Figure 3 Snapshots of 8<sup>+</sup>G1 complexed with RNA at 18 ns from different starting position:  
a) 8<sup>+</sup>G1 in the minor groove of RNA; b) 8<sup>+</sup>G1 in the major groove of RNA.

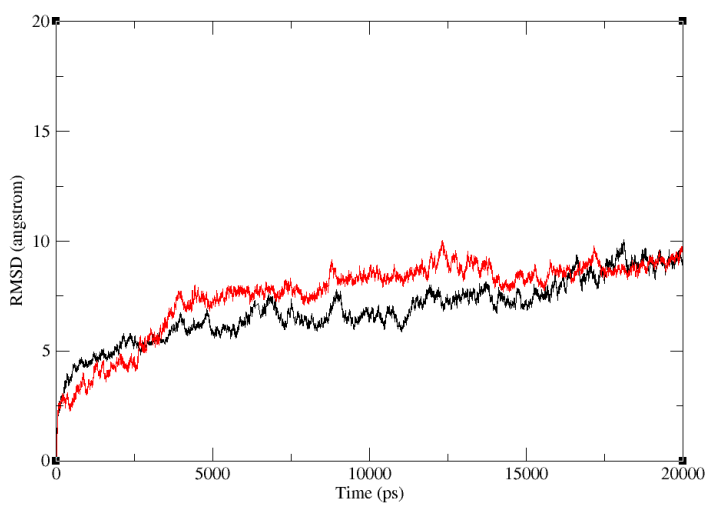


Figure 4 RMSD versus time for 14+G1-RNA complexation over the 20 ns simulations. The RMSD is mass weighted for polymer-RNA complexes, with water and counter-ions not included. Black line is the 14+G1 complexed with RNA with starting position adjacent to the major groove. Red line (lower curve light) is the 14+G1 complexed with RNA with starting position adjacent to the minor groove.

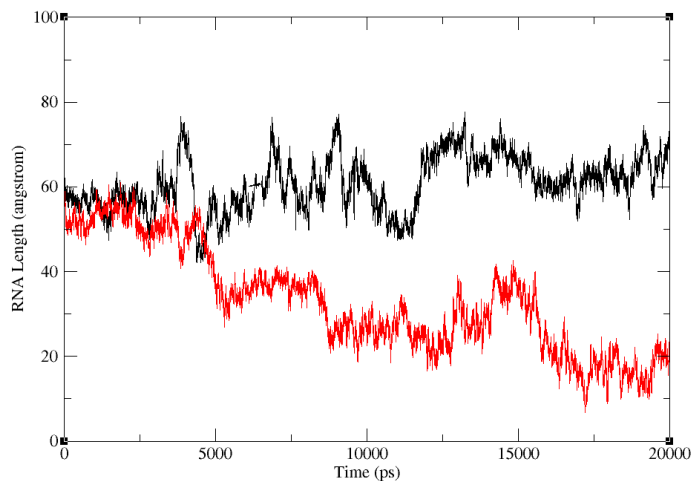


Figure 5. RNA length (end-to-end) as a function of time for complexation between 14+G1 and RNA during the 20 ns simulations. Line definitions as for Figure 4 above.

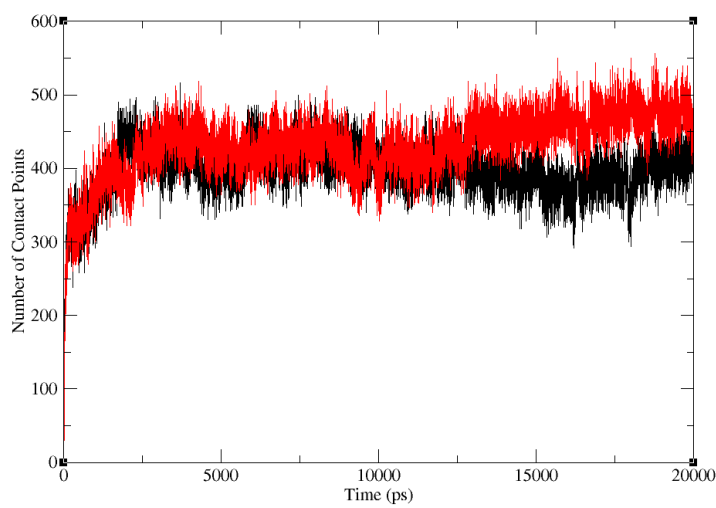
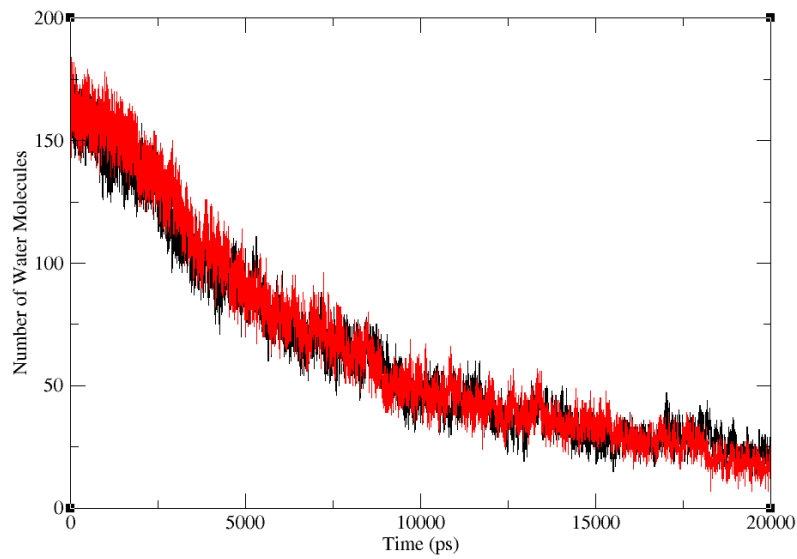


Figure 6. Variation of the number of contact points between 14+G1 and RNA (any contact within 3 Å) during the 20 ns simulations. Line definitions as for Figure 4 above.

a)



b)

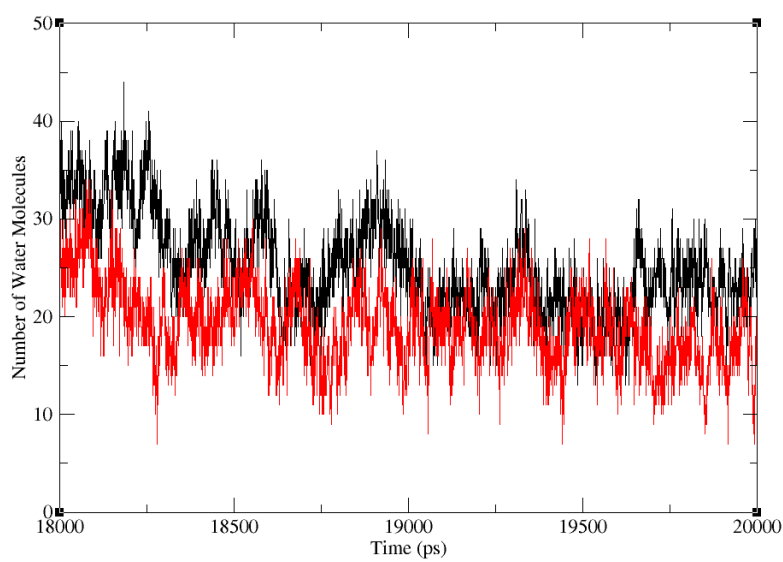


Figure 7. Number of water molecules in a spine of hydration (any contact within 3 Å of the polymer) as a function of time for complexation between 14+G1 and RNA during the 20 ns simulations. Figure 7a shows the behavior over the whole 20 ns, while Figure 7b shows late-time behavior during the last 2 ns. Line definitions as for Figure 4 above.

Table 1 Simulation cell compositions and atom numbers for the systems of cationic polymers-siRNA complexation

	14 <sup>+</sup> G1-RNA complex		8 <sup>+</sup> G1–RNA complex		6 <sup>+</sup> G0–RNA complex		4 <sup>+</sup> G0–RNA complex	
	Major groove	Minor groove	Major groove	Minor groove	Major groove	Minor groove	Major groove	Minor groove
Atom number of RNA	1335	1335	1335	1335	1335	1335	1335	1335
Atom number of polymers	242	242	236	236	60	90	88	88
Number of Na <sup>+</sup>	26	26	32	32	34	34	36	36
Molecule number of water	11080	10774	9025	8805	10997	10660	8764	8694
Total atom number	34843	33925	28678	28018	34450	33439	27751	27541

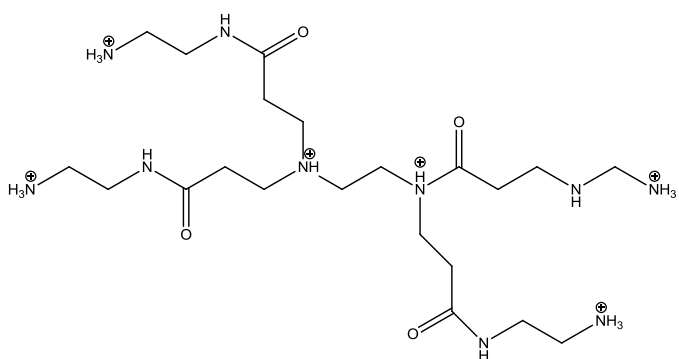
Table 2 Binding free energies for polymer-RNA complex in the minor or major groove using the MM-PBSA method

	14 <sup>+</sup> G1 -RNA complex		8 <sup>+</sup> G1–RNA complex		6 <sup>+</sup> G0–RNA complex		4 <sup>+</sup> G0–RNA complex	
	Major groove	Minor groove	Major groove	Minor groove	Major groove	Minor groove	Major groove	Minor groove
$\Delta E_{elec}$	-11112.30	-11007.47	-5742.27	-5771.37	-5292.97	-5196.57	-3273.51	-3020.98
(kcal/mol)	(62.87)	(52.09)	(52.80)	(58.76)	(38.72)	(31.18)	(67.44)	(78.06)
$\Delta E_{vdW}$	-60.02	-65.44	-49.57	-51.87	-23.64	-37.56	-18.06	-18.00
(kcal/mol)	(5.37)	(6.72)	(4.05)	(4.41)	(3.11)	(4.71)	(3.77)	(4.43)
$\Delta E_{MM}$	-11172.32	-11072.91	-5791.84	-5823.24	-5316.61	-5234.13	-3291.58	-3038.98
(kcal/mol)	(63.45)	(51.18)	(52.17)	(59.27)	(38.56)	(30.35)	(69.11)	(81.10)
$\Delta\Delta G_{np}$	-13.43	-14.28	-9.72	-10.54	-6.89	-7.58	-5.03	-4.83
(kcal/mol)	(0.39)	(0.23)	(0.33)	(0.20)	(0.16)	(0.21)	(0.43)	(0.73)
$\Delta\Delta G_{PB}$	10976.04	10848.36	5673.26	5719.02	5238.46	5128.83	3248.38	2983.87
(kcal/mol)	(63.68)	(49.32)	(51.27)	(58.64)	(36.84)	(28.62)	(64.72)	(78.55)
$\Delta\Delta G_{solv}$	10962.61	10834.08	5663.54	5708.49	5231.57	5121.25	3243.35	2979.05
(kcal/mol)	(63.41)	(49.27)	(51.14)	(58.57)	(36.81)	(28.60)	(64.33)	(77.89)
$\Delta\Delta G_{elec}$	-136.26	-159.11	-69.02	-52.34	-54.50	-67.74	-25.14	-37.11
(kcal/mol)	(8.43)	(9.39)	(6.52)	(9.07)	(4.54)	(7.69)	(5.36)	(4.61)
$\Delta G_{bind}$	<b>-209.71</b>	<b>-238.83</b>	<b>-128.30</b>	<b>-114.75</b>	<b>-85.04</b>	<b>-112.88</b>	<b>-48.23</b>	<b>-59.94</b>
(kcal/mol)	(5.76)	(6.48)	(5.11)	(6.95)	(3.30)	(5.34)	(5.84)	(5.13)

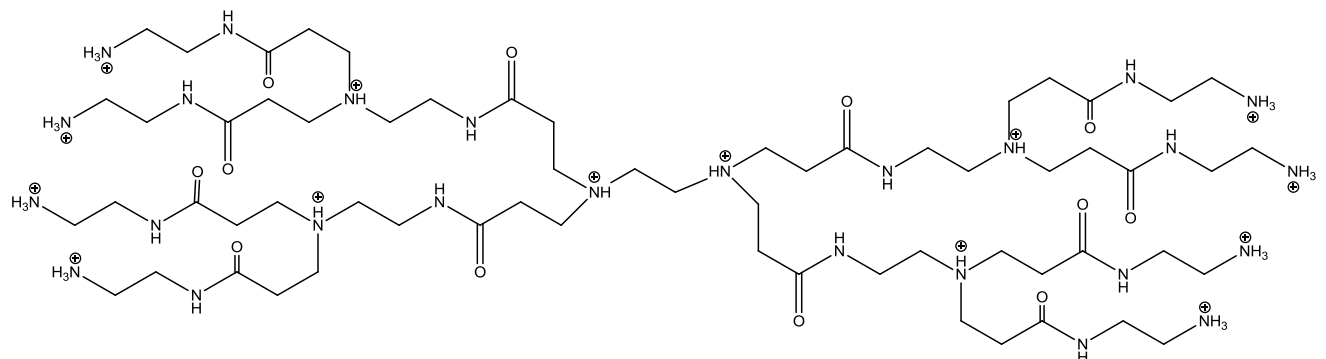
Note:

1. The major (or minor) groove refers to the starting structure of the complex, not the final structure.
2. Average over 200 snapshots from the last 2 ns trajectory; standard error of the mean in parentheses.
3. Definition of energy contributions:  $\Delta E_{elec}$ , electrostatic molecular mechanical energy;  $\Delta E_{vdW}$ , van der Waals molecular mechanical energy;  $\Delta E_{MM} = \Delta E_{elec} + \Delta E_{vdW}$ ;  $\Delta\Delta G_{np}$ , nonpolar solvation energy;  $\Delta\Delta G_{PB}$ , electrostatic solvation energy;  $\Delta\Delta G_{solv} = \Delta\Delta G_{np} + \Delta\Delta G_{PB}$ ;  $\Delta\Delta G_{elec} = \Delta E_{elec} + \Delta\Delta G_{PB}$ ;  $\Delta G_{bind}$ , calculated binding energy.

## Supplementary Materials



a) Six positive-charged G0-PAMAM dendrimer ( $6^+$ dendrimer);



b) Fourteen positive-charged G1-PAMAM dendrimer ( $14^+$ dendrimer);

Figure S-1 Chemical structures of polymers.

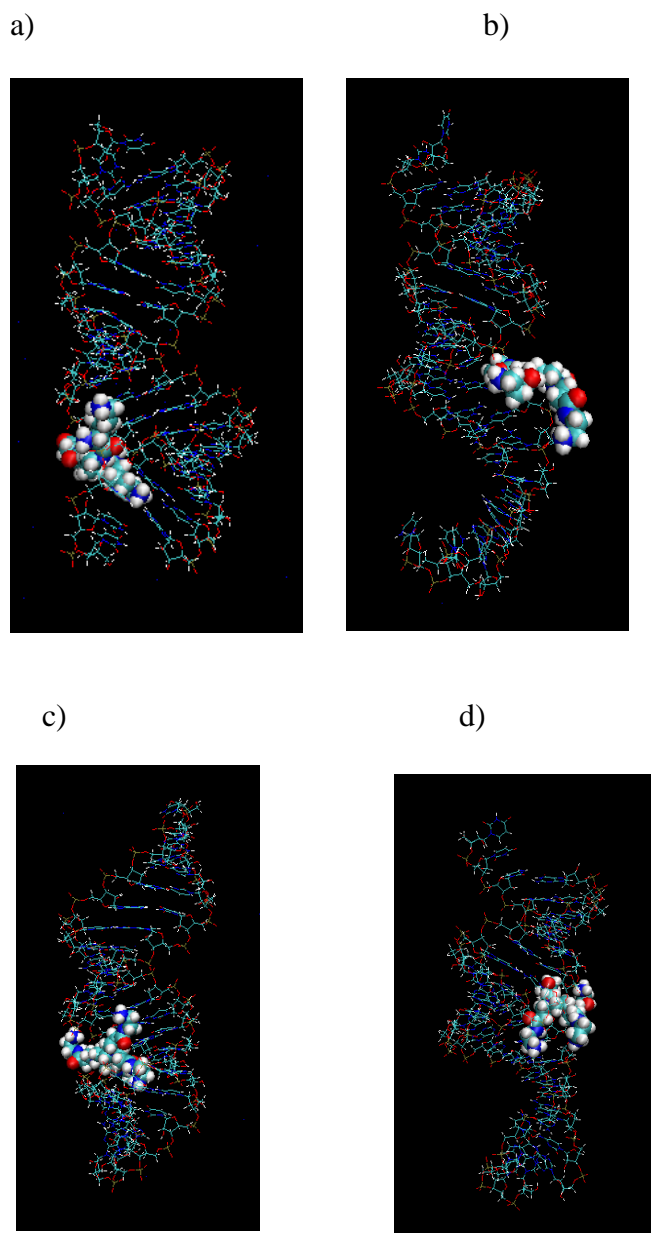


Figure S-2 Snapshots of  $4^+G0$  and  $6+G0$  complexed with RNA from different starting position: a)  $4^+G0$  in the minor groove of RNA at 18 ns; b)  $4^+G0$  in the major groove of RNA at 18 ns; c)  $6+G0$  in the minor groove of RNA at 20 ns; d)  $6+G0$  in the major groove of RNA at 20 ns.

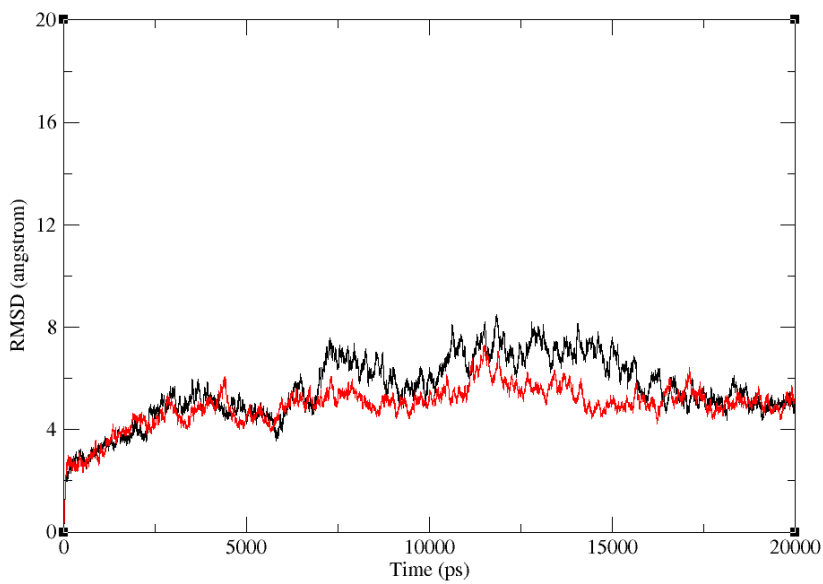


Figure S-3 RMSD versus time for 6+G0-RNA complexation over the 20 ns simulations, shown for the cases where the dendrimer start out adjacent to the major groove. The RMSD is mass weighted for polymer-RNA complexes, with water and counter-ions not included. Black line is the 6+G0 complexed with RNA with starting position adjacent to the major groove. Red line (lower curve light) is the 6+G0 complexed with RNA with starting position adjacent to the minor groove.

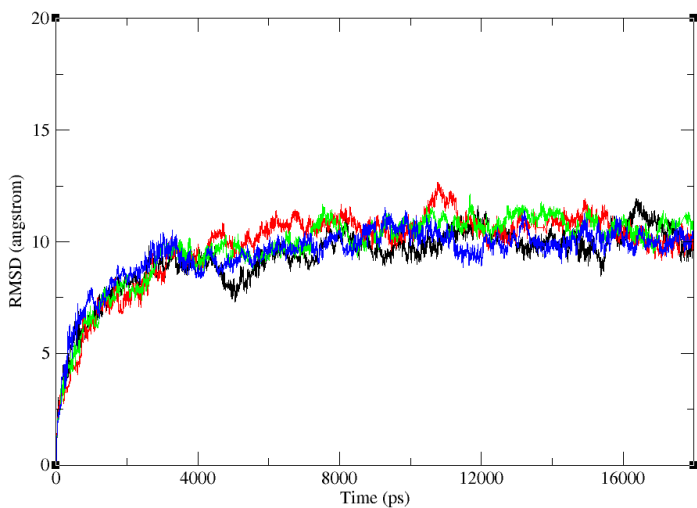


Figure S-4 RMSD versus time of dendrimer-RNA complexation in 18 ns at neutral pH. RMSD is mass weighted for polymer-RNA complex without water and counterions. Black line is 4<sup>+</sup>G0 complexed with RNA at the starting position of the major groove; red line is 4<sup>+</sup>G0 complex RNA at the starting position of the minor groove; green line is 8<sup>+</sup>G1 complex RNA at the starting position of the major groove; blue line is 8<sup>+</sup>G1 complex RNA at the starting position of the major groove.